CHAPTER 3

Co-Cr Substituted $SrFe_{12-x-y}Co_xCr_yO_{19}$ Series

3.1 Introduction

Strontium hexaferrite is the world's largest traded magnet due to its decent magnetic characteristics and stability in processing cost (de Julián Fernández et al., 2021). Their magnetic characteristics are tunable by the effective substitution of the different elements, where superexchange interactions between Fe-O are responsible for the magnetic tunability. In order to improve the magnetic properties of SrM, Co-Cr substitution at the Fe lattice site is studied in this chapter. A composition of $SrFe_{12-x-y}Co_xCr_yO_{19}$ (x, y = 0,0; 0,1; 0.25,0.75; 0.50,0.50; 0.75,0.25; 1,0) is ascertained here. The substitutional effect of Co-Cr is not studied yet in the SrM. From the literature review, it is evident that Co ion is a significant element for high M_s value in SrM (Liu et al., 2012; Roohani et al., 2017; Xie et al., 2012), but it may change the magnetic nature of SrM towards soft magnetism. So, Cr substitution is also selected here to retain the hard magnetic characteristics of SrM because it is reported to be effective in H_c improvement (Fang et al., 2005; Katlakunta et al., 2015; Slimani et al., 2018). In this chapter, the possibilities of enhancing magnetic properties in strontium hexaferrite have been studied.

3.2 Results and Discussion

3.2.1 TG/DTA Analysis

Fig. 3.1 shows the TG/DTA curve of the $SrFe_{12}O_{19}$ dried gel precursor. The TG curve shows 14% weight loss in the temperature region 80°C-200°C due to decomposing a small amount of nitrates and citric acid complex. Further significant weight loss of 68% in the region of 200°C-240°C represents the evaporation of residual solvent and crystallization

process. There are two endothermic peaks in the DTA curve. The two exothermic peaks in the region 190°C-290°C and 290°C-390°C signify the combustion of citric acid and the complete decomposition of organic material. It is recognized as the thermally prompted redox reaction of gel precursor where NO_3 ions act as oxidants, and chelating agent (citric acid) acts as a reductant with CO_2 and NO_χ gas emission (Masoudpanah & Seyyed Ebrahimi, 2013) according to Eq. (3.1). The exothermic peak in the region 290°C-390°C mainly represents the complete thermal decomposition and simultaneous crystallization reaction of strontium hexaferrite (Sang Won Lee et al., 2003).

$$Sr(NO_3)_2 + 12\ Fe(NO_3)_3.9H_2O + C_6H_8O_7 + NH_4OH \xrightarrow{\Delta} SrFe_{12}O_{19} + NH_3\uparrow + CO_2\uparrow + NO_\chi\uparrow + H_2O \quad (3.1)$$

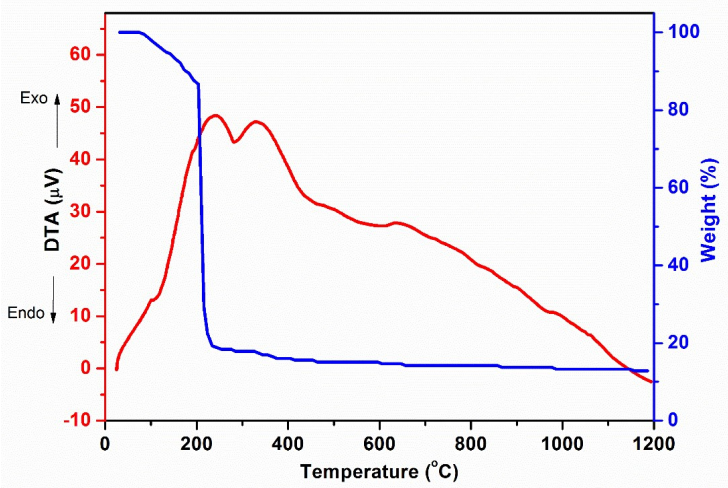

Figure 3.1 *TG/DTA curve of $SrFe_{12}O_{19}$ dried sol-gel.*

3.2.2 Structural Properties

Fig. 3.2 shows the XRD patterns of $SrFe_{12-x-y}Co_xCr_yO_{19}$ ($0 \leq x, y \leq 1$) calcined ferrite powders. The hexagonal SrM phase is identified for all the compositions with the absence of any secondary or impurity phases in the determination limits. All the characteristic diffraction peaks have confirmed the formation of the hexagonal phase with a space group of $P6_3/mmc$, and are indexed according to the ICDD card 79-1412 (Liu et

al., 2013). The higher peak intensity of (107) plane than the pure SrM sample suggests that the Co/Cr content excites the hexaferrite formation, and the favored direction is parallel to the *c*-axis along the (107) plane. The structural properties such as lattice parameters (*a* and *c*), *c/a* fraction, cell volume (*V*), crystallite size (*D*), strain (ϵ), and x-ray density (χD) are given in Table 3.1.

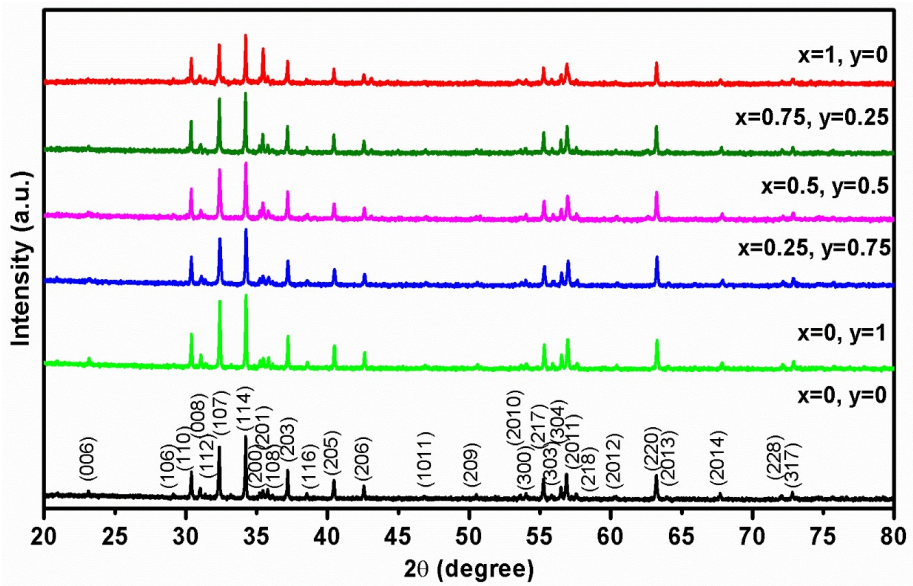

Figure 3.2 *XRD patterns of calcined $SrFe_{12-x-y}Co_xCr_yO_{19}$ ($0 \leq x, y \leq 1$) hexaferrites.*

A slight discrepancy in lattice parameters is observed due to the difference in ionic radius of Fe^{3+} (0.64 Å), Co^{3+} (0.63 Å) (Nathiya et al., 2012), and Cr^{3+} (0.63 Å) (Huang et al., 2015). The substitution of Co/Cr at Fe site gives a resultant change in ionic radius Δr = -0.01 Å, and it causes a small reduction in *c* parameter. Lattice parameter *a* increases marginally, while the variation in the *c* parameter is steeper in comparison to the pristine SrM. It indicates a change in the easy demagnetization axis. Since ionic radii are almost equal, the variation in lattice parameters may be accredited by modification of exchange energy due to the substitution (Fang et al., 2005). Co and Cr ions preferably possess the octahedral site. Accordingly, Cr^{3+} [1.2 Δ_o (↑/↓)] and/or Co^{3+} [0.0 Δ_o (↑) / 2.0 Δ_o (↓)] ion substitution at Fe^{3+} [0.0 Δ_o (↑) / 2.0 Δ_o (↓)] site result in the anisotropic deviation in the

lattice parameters by relative change in the net field energy (Praveena et al., 2015). The *c/a* ratio is less than 3.98, which confirms the formation of M-type hexagonal magnetoplumbite structure and indicates large crystalline anisotropy for all the compositions (Pullar, 2012). Lattice strain is approximately unchanged due to almost equal ionic radii of the substituted ions. Crystallite size is observed in the range of 59.97-60.33 nm, which confirms the formation of single-domain particle size for all the samples as *D* values are less than critical size ~500 nm (derived from Kittle's theory for single domain creation (Luo et al., 2012).

Table 3.1 *Structural parameters of $SrFe_{12-x-y}Co_xCr_yO_{19}$ ($0 \leq x, y \leq 1$) hexaferrites.*

Composition	Lattice Parameter		*c/a*	*V*	*D*	ϵ	χD
	a, b (Å)	*c* (Å)		(Å^3)	(nm)	(10^{-2})	(g/cm^3)
x=0, y=0	5.85	23.07	3.94	683.74	60.33	0.19	5.15
x=0, y=1	5.87	23.00	3.92	686.33	60.04	0.21	5.11
x=0.25, y=0.75	5.87	23.00	3.92	686.33	60.03	0.21	5.12
x=0.5, y=0.5	5.88	23.00	3.91	688.67	60.00	0.21	5.12
x=0.75, y=0.25	5.88	23.02	3.91	689.27	60.02	0.21	5.12
x=1, y=0	5.88	23.04	3.92	689.87	59.97	0.19	5.13

3.2.3 Spectroscopic Properties

Fig. 3.3 shows the infrared spectra of $SrFe_{12-x-y}Co_xCr_yO_{19}$ ($0 \leq x, y \leq 1$) calcined powders in the range of 4000-400 cm^{-1}. Spectral analysis delivers detailed statistics of intermediate structural changes due to calcination. In all the compositions, there is the presence of three characteristic absorption band ν_3 (432-450 cm^{-1}), ν_2 (549-559 cm^{-1}), and ν_1 (598-602 cm^{-1}). Absorption band 400-500 cm^{-1} is attributed to intrinsic vibration at the octahedral site while 500-700 cm^{-1} to the tetrahedral site (Baniasadi et al., 2014). The appeared bands are in an acceptable range to the reported SrM analysis and confirm the formation of M-type hexaferrite structure (Xie et al., 2018). The wavenumber ν_3 (octahedral) is associated with the Fe-O bending by $Fe\text{-}O_4$ and Fe-O stretching by $Fe\text{-}O_6$.

The wavenumber ν_2 and ν_1 (tetrahedral; large owing to shorter bond length (Yang et al., 2018)) are resulted from Fe-O stretching by Fe-O_4 (Carol Trudel et al., 2019).

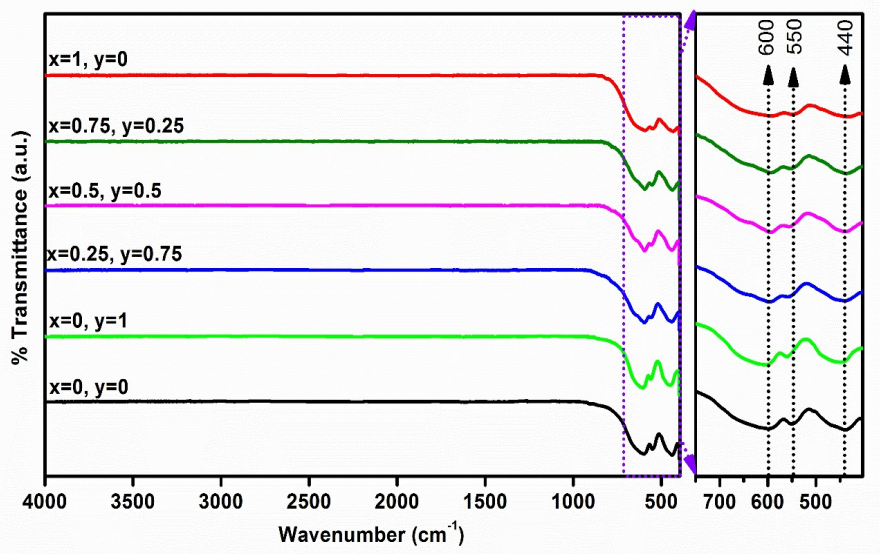

Figure 3.3 *FT-IR spectra of calcined $SrFe_{12-x-y}Co_xCr_yO_{19}$ ($0 \leq x, y \leq 1$) hexaferrites.*

Table 3.2 *Characteristic absorption peaks [ν_1, ν_2 (tetrahedral) & ν_3 (octahedral)] and bond length (r) of $SrFe_{12-x-y}Co_xCr_yO_{19}$ ($0 \leq x, y \leq 1$) hexaferrites.*

Composition	ν_1 (cm^{-1})	r_1 (Å)	ν_2 (cm^{-1})	r_2 (Å)	ν_3 (cm^{-1})	r_3 (Å)
x=0, y=0	598	4.41	553	4.64	441	5.4
x=0, y=1	600	4.40	555	4.63	450	5.33
x=0.25, y=0.75	598	4.41	553	4.64	440	5.41
x=0.5, y=0.5	598	4.41	553	4.64	439	5.42
x=0.75, y=0.25	598	4.41	550	4.66	435	5.45
x=1, y=0	598	4.41	550	4.66	432	5.47

Wave numbers are conversely related to the atomic weight according to Hooke's law, which results in the variation of *v* as listed in Table 3.2. Hooke's law demonstrates that the wavenumber is inversely proportional to the atomic weight of molecules. Co (= 58.93 g/mol) ion is heavier than Fe (= 55.85 g/mol) ion. Subsequently, it causes the shifting of peaks towards a lower wavenumber. Cr (= 52 g/mol) ion is lighter than Fe ion; hence shifting of characteristic peaks is observed towards the higher wavenumber (Ghezelbash et

al., 2018). The resilient and sharper characteristic peaks depict the strengthening of chemical polarization of internal chemical bonds by Co-Cr substitution. It indicates the successful substitution of Co-Cr ions in the SrM structure.

3.2.4 Densification and Microstructural Properties

The densification properties of all samples are estimated by Archimedes' methodology. The bulk density (*BD*) and porosity (*P*) are listed in Table 3.3. Density of all samples has shown an enhanced densification behavior with Co ion content. However, the sample containing only Cr ion shows a decreasing density behavior. The lower *BD* than the χD suggests the presence of pores, which are formed during the fabrication and firing of samples causing irregular grains and porosity in samples.

Table 3.3 *Atomic weight %, average grain size (G_{avg}), bulk density (BD), and porosity (P) of $SrFe_{12-x-y}Co_xCr_yO_{19}$ ($0 \leq x, y \leq 1$) hexaferrites.*

Composition	Atomic weight %					G_{avg}	*BD*	Porosity
	Sr	Fe	Cr	Co	O	(µm)	(g/cm^3)	(%)
x=0, y=0	8.11	63.02	-	-	28.87	0.64	3.88	24.66
x=0, y=1	8.13	58.01	4.90	-	28.96	1.11	3.44	32.68
x=0.25, y=0.75	8.12	57.86	3.65	1.34	29.03	3.44	4.53	11.52
x=0.5, y=0.5	8.11	57.80	2.42	2.71	28.96	3.50	4.70	8.20
x=0.75, y=0.25	8.10	57.67	1.23	4.20	28.80	4.13	4.74	7.42
x=1, y=0	8.08	57.56	-	5.60	28.76	7.84	4.87	5.07

All SEM micrographs of sintered $SrFe_{12-x-y}Co_xCr_yO_{19}$ ($0 \leq x, y \leq 1$) samples are shown in Fig. 3.4. These micrographs confirm the formation of hexagonal structure in the samples. Chemical compositions are confirmed by EDS spectroscopy, and the atomic weight percentages of elements are listed in Table 3.3. It is found that both Co and Cr ions promote grain growth due to the exothermic redox reaction (Roohani et al., 2017). In the Cr substituted sample, the grain growth may be explained by the eminent fact of high

sintering temperature, which causes the grain growth of properly oriented grains at the expense of disoriented ones (Rhein et al., 2018) and hence, results in the declining density. Whereas, in Co-substituted samples, intense grain growth is experienced as a result of the partial liquid-phase-assisted sintering process (Johnson et al., 2010), causing a proportional increase in the grain size and the densification of the sample. A rich Co content ($x \geq 0.75$) can abruptly increase the average grain size. (Wu et al., 2017) have also observed an abnormal growth of grains with increasing Co substitution. It may be due to the lower melting temperature of Co (1768K) than Cr (2150K). It may also be resulted due to the smaller binding energy of Co-O than that of Fe-O, which increases the average grain size with the increasing Co ion content (Wu et al., 2017).

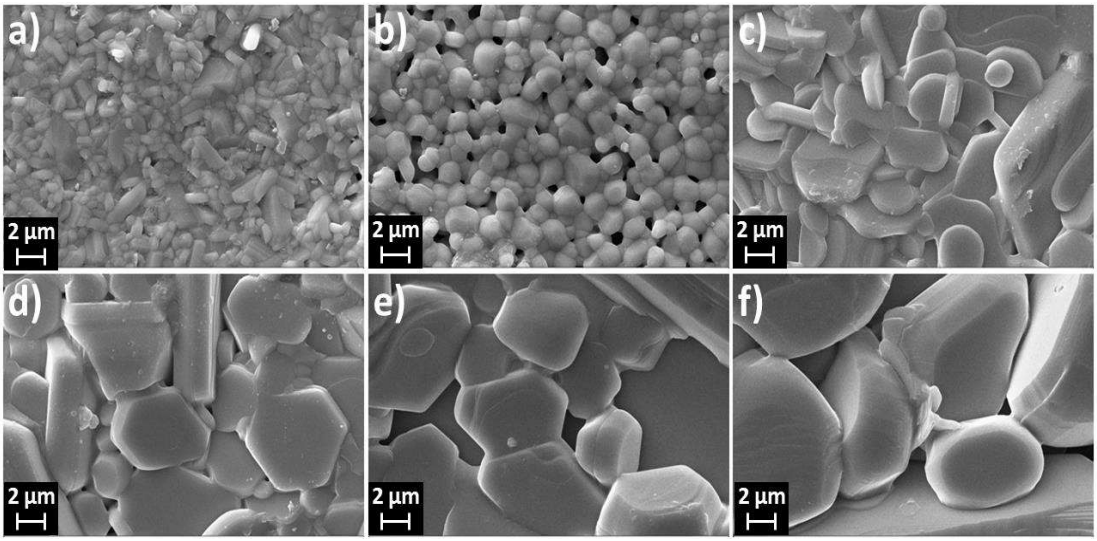

Figure 3.4 *SEM micrographs of a) $SrFe_{12}O_{19}$, b) $SrFe_{11}CrO_{19}$, c) $SrFe_{11}Co_{0.25}Cr_{0.75}O_{19}$, d) $SrFe_{11}Co_{0.5}Cr_{0.5}O_{19}$, e) $SrFe_{11}Co_{0.75}Cr_{0.25}O_{19}$, and f) $SrFe_{11}CoO_{19}$ hexaferrites.*

3.2.5 Magnetic Properties

Fig. 3.5 shows the *M-H* curve of $SrFe_{12-x-y}Co_xCr_yO_{19}$ ($0 \leq x, y \leq 1$) hexaferrites at 300 K. From these curves, the values of saturation magnetization (M_s), remanent magnetization (M_r), coercivity (H_c), squareness ratio (M_r/M_s), H_a, and K_{eff} are extracted and listed in Table 3.4. The value of M_s is observed in the range of 59.89-71.18 emu/g, and H_c

varies between 3.23 Oe-6.26 kOe. The squareness ratio (M_r/M_s) is found to be less than 0.5, which represents the formation of the multi-magnetic domain (Yasmin et al., 2019).

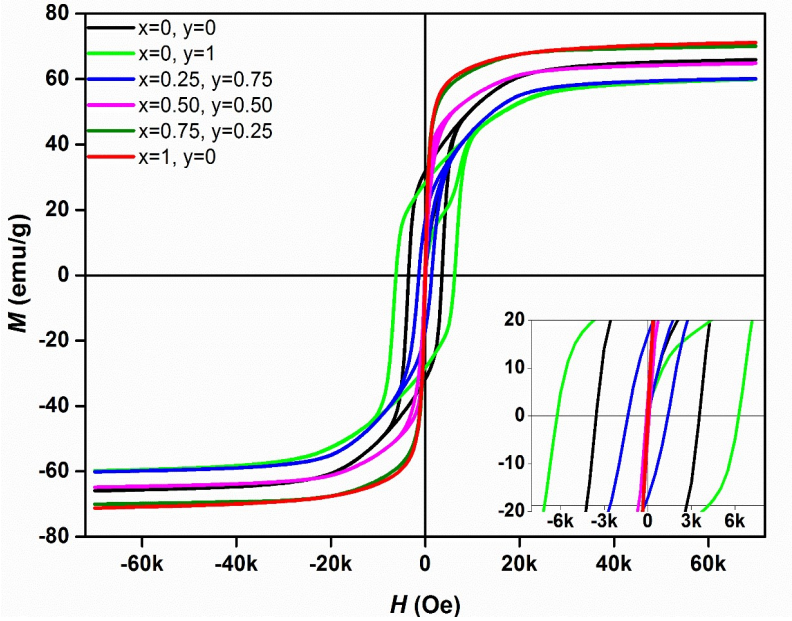

Figure 3.5 *M-H hysteresis curve of $SrFe_{12-x-y}Co_xCr_yO_{19}$ ($0 \leq x, y \leq 1$) hexaferrites.*

M_s is an intrinsic property of the material, whereas M_r and H_c are the extrinsic properties. Remanence (M_r) is observed to decrease with both Co and Cr ion substitution. It strongly depends on chemistry, density, and orientation. A decreasing trend of M_r with Cr ion may be caused due to the decrease in density (Nourbakhsh et al., 2011). M_r variation trend due to Co ion may have resulted from high processing temperature (Wu et al., 2017). M_s is found in correlation with the Bohr magnetron (μ_B). Co ion substitution causes an increase in M_s, while the substitution of Cr ion causes a slight decrease in M_s. The reported studies suggest that the occupying tendency of Cr ion is in the 12*k* (↑), 2*a* (↑), and $4f_2$ (↓) lattice site (Slimani et al., 2018) whereas, Co ion prefers $4f_2$ (↓) site mainly (Yang et al., 2018). With Co ($4\mu_B$) ion substitution at Fe ($5\mu_B$) site, the net magnetic moment in down-spin direction decreases, and hence a significant increase in M_s is experienced. Cr ($3\mu_B$) ion substitution mainly prefer 12*k* and 2*a* site and cause a diminution of the net magnetic

moment in up-spin direction, thereby resulting in decline of M_s value. In the multi-domain structure, grain growth causes to decrease the anisotropic field and increase in the M_s. It is well known that M_s of the ferrite increases with improving the grain size and bulk density. Improvement in M_s with Co content is primarily responsible to the improvement in bulk density, which not only causes a decrease of the demagnetizing field due to porosity reduction but also improves the spin rotational contribution, which increases the M_s (Shrotri et al., 1999).

Table 3.4 *Saturation magnetization (M_s), remanent magnetization (M_r), squareness ratio (M_r/M_s), coercivity (H_c), magnetocrystalline anisotropy field (H_a), and effective magnetic anisotropy (K_{eff}) of $SrFe_{12-x-y}Co_xCr_yO_{19}$ ($0 \leq x, y \leq 1$) hexaferrites at 300 K.*

Composition	M_s (emu/g)	M_r (emu/g)	$\frac{M_r}{M_s}$	μ_B	H_c (Oe)	H_a (kOe)	K_{eff} (10^5 erg/g)
$SrFe_{12}O_{19}$	65.94	31.77	0.48	12.54	3550.50	17.73	5.84
$SrFe_{11}CrO_{19}$	59.89	28.37	0.47	11.34	6256.06	21.03	6.30
$SrFe_{11}Co_{0.25}Cr_{0.75}O_{19}$	60.11	17.04	0.28	11.40	1383.50	17.77	5.34
$SrFe_{11}Co_{0.50}Cr_{0.50}O_{19}$	64.82	3.95	0.06	12.32	99.22	14.28	4.63
$SrFe_{11}Co_{0.75}Cr_{0.25}O_{19}$	70.08	2.13	0.03	13.34	36.21	12.97	4.54
$SrFe_{11}CoO_{19}$	71.18	1.44	0.02	13.57	3.23	12.23	4.35

Rich Cr ion concentration promotes the energy barrier by dissipating a large amount of energy at the domain wall (Huang et al., 2015). It escalates domain wall displacement resistance and results in higher coercivity (6.26 kOe) for $SrFe_{11}CrO_{19}$. With rising Co ion concentration, different exchange interaction arises, like Fe-O-Fe, Fe-O-Co, and Co-O-Co, and all of them favor ferromagnetism (Mehmood et al., 2017). Due to Co substitution, iron ion exchange is uncoupled and prompts easier flipping of magnetic moments. It is reflected in all x > 0 samples, causing a drastic drop in H_c value. The coercivity (H_c) parameter and magnetocrystalline anisotropy field (H_a) parameter exhibits a direct proportionality relationship. Variation in H_c has followed the same relationship,

i.e., proportional to the H_a and K_{eff}, which can be visualized in Table 3.4. Both effective magnetocrystalline anisotropy (K_{eff}) and magnetocrystalline anisotropy field (H_a) are estimated by Eq. (2.14) [$K_{eff} = M_s\sqrt{(15\gamma/4)} = M_s H_a/2$] (Almessiere et al., 2019), which is resulted from the Stoner-Wohlfarth (S-W) theory. The slope of S-W fitting gives γ through the M vs. $1/H^2$ plot, as shown in Fig. 3.6.

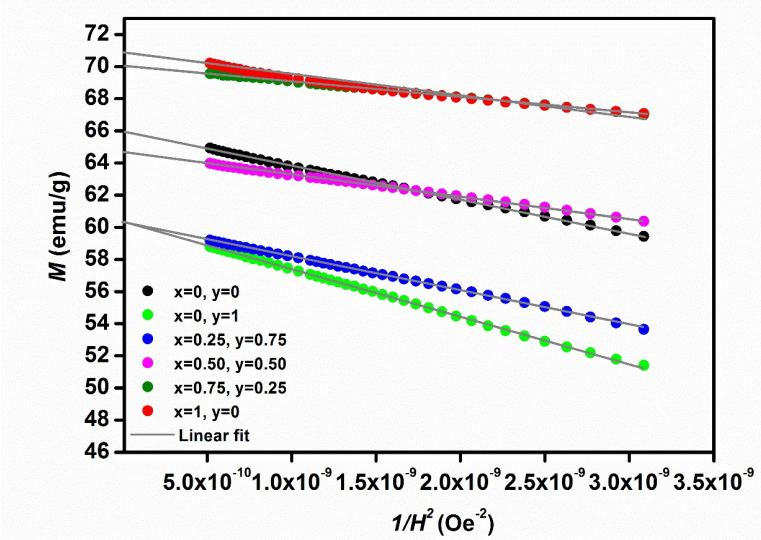

Figure 3.6.*M vs. $1/H^2$ plot with S-W linear fitting for $SrFe_{12-x-y}Co_xCr_yO_{19}$ ($0 \leq x, y \leq 1$) hexaferrites.*

Occupying preference of Co ion at the $4f_2$ site may cause a reduction in the uniaxial magnetocrystalline anisotropy (Zhang et al., 2019). It causes a decrease in H_c due to the gradual change of magnetic anisotropy from uniaxial to planar till $x \leq 0.75$. With further increase in x, the easy axis of magnetization fell over the basal plane leading to a nearly planar magnetic anisotropy (Zhang et al., 2019), therefore resulting in the obtained H_c variation. Related H_c dilution due to Co substitution is also experienced by (Roohani et al., 2017). Such a hard to soft magnetic transition may explain by the exchange interaction between Fe-Fe ions, which are dominated by the exchange interaction of Fe-Co ions that can reduce the nucleation field and results in low H_c. H_c has also been considerably affected by grain size. Bigger the grain size lesser the grain boundaries, which act as a pinning site

for the domain wall movement. As the Co content increased, the grain size became bigger. The reverse magnetic field of the demagnetization can be reduced with domain rotation, where the bigger grain sizes have more domain wall movement. As a result, low coercivity is observed for the bigger grain size. It may also be due to the presence of the internal demagnetization field because of the soft magnetic nature of Co ion (Liu et al., 2012; Zhang et al., 2019). During the application of the demagnetization field, domain-wall motion and domain rotation reverse the hard moment by the exchange coupling phenomenon, which results in a reduction of coercivity (Torkian & Ghasemi, 2019).

3.2.6 Dielectric Properties

Dielectric properties are helpful in understanding the conduction mechanism of electric charge. The typical frequency-dependent dielectric constant behavior of $SrFe_{12-x-y}Co_xCr_yO_{19}$ ($0 \leq x, y \leq 1$) hexaferrites is shown in Fig. 3.7. The dielectric parameters, dielectric constant (ε) and tangent dielectric loss ($\tan\delta$), of all the compositions at 1 MHz frequency are listed in Table 3.5. Here, a high value of ε (861) is attained for pure SrM. The observed behavior of ε is similar to the ferrite materials and can be explained by Koop's and Maxwell Wagner's theory (Chauhan et al., 2018; Shakoor et al., 2014). According to these theories, there are two structural layers: first is conducting layers (made up of large ferrite grains), and second is a poor conducting layer (grain boundaries). During the conduction process, the electrons move towards the grain boundaries through hopping and result in high resistance, i.e., they oppose conduction.

With the substitution of Co-Cr ions, it decreases according to the grain size variation, which helps in the conduction mechanism resulting in low ε in the substituted samples. A decreasing pattern of dielectric constant is observed with the increasing frequency and substitution amount. A decline in ε is more notable at lower frequencies, while it becomes nearly constant at higher frequencies. A decrease in ε with frequency is caused by the

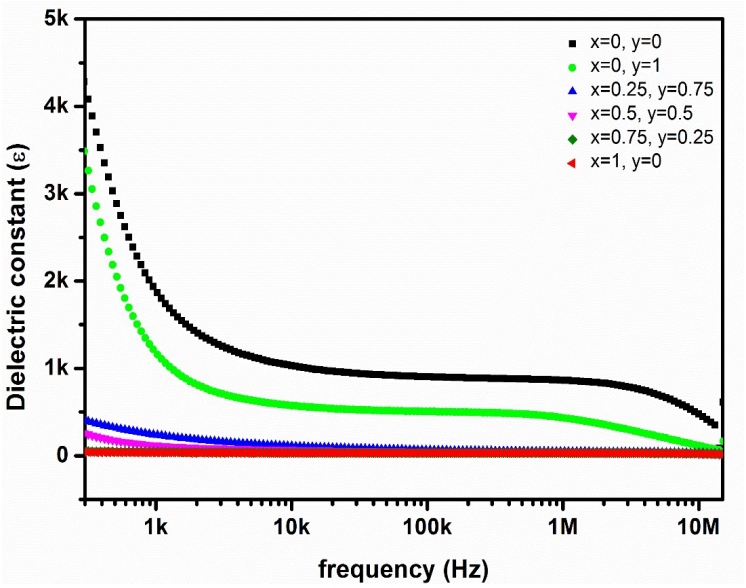

Figure 3.7 *Dielectric constant (ε) of $SrFe_{12-x-y}Co_xCr_yO_{19}$ ($0 \leq x, y \leq 1$) hexaferrites with respect to frequency at room-temperature.*

Table 3.5 *Room-temperature value of dielectric constant (ε), tangent loss (tanδ), resistivity (ρ) and conductivity (σ) of $SrFe_{12-x-y}Co_xCr_yO_{19}$ ($0 \leq x, y \leq 1$)hexaferrites at 1MHz frequency.*

Composition	ε	$tan\delta$	ρ (10^6 Ω-cm)	σ (10^{-7} S-cm^{-1})
x=0, y=0	861.12	0.098	2.07	3.50
x=0, y=1	432.46	0.297	1.36	1.54
x=0.25, y=0.75	46.58	0.192	19.55	2.02
x=0.5, y=0.5	36.99	0.144	32.73	1.18
x=0.75, y=0.25	31.49	0.014	377.82	1.11
x=1, y=0	29.94	0.006	936.56	0.57

polarization mechanisms. With the substitution of Co and Cr, the formation of Fe^{2+} ions takes place at the octahedral site as both preferentially occupy that site. Electron hopping at this site follows the applied field at low frequencies. It leads to charge displacement and electron batching at poorly-conducting grain boundaries, causing a higher value of ε at lower frequencies (Praveena et al., 2015). According to the variation in the electric field, electron exchange between charge carriers cannot occur because of a short relaxation time at higher frequencies due to orientational polarization (Praveena et al., 2015). It obstructs

the movement of charge carriers towards non-conducting grain boundaries, which reduces the polarization effect. Hence, electron hopping could not follow the applied field, but it lags with increasing frequency and causes a decrease in ε, as shown in Fig. 3.7. The polarization is mainly governed by the space charge (SC) polarization that is contributed by the conductivity of the material, space charge carriers, and hopping exchange of the charges, which are controlled by the resultant displacement of these charges with the field and the density of the localized states. The addition of Co-Cr ions to the SrM structure causes a decrease of Fe ions at the octahedral site. Octahedral lattice sites are mainly responsible for the space charge polarization and the hopping exchange of the charges. Therefore, ε is found to reduce with Co-Cr content due to the reduction in the hopping and polarization mechanism.

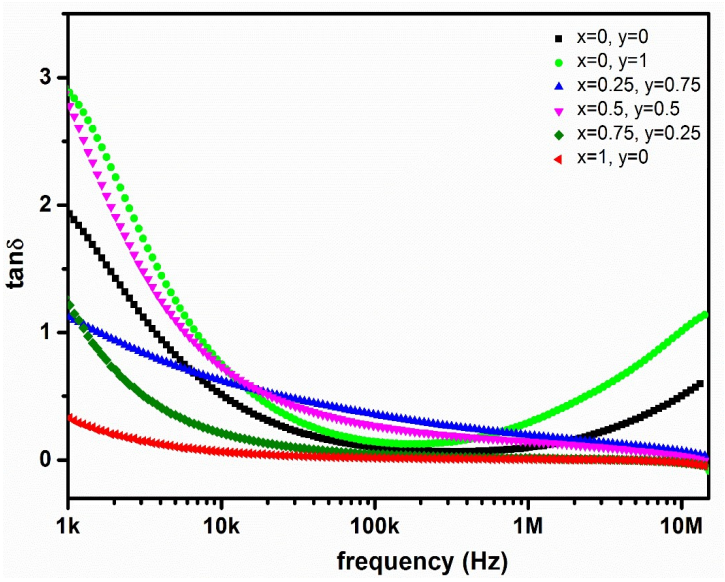

Figure 3.8 *Dielectric loss (tanδ) of $SrFe_{12-x-y}Co_xCr_yO_{19}$ ($0 \leq x, y \leq 1$) hexaferrites with respect to frequency at room-temperature.*

Dielectric loss (tanδ) depends on the processing parameters and heat treatment process. It is found in decreasing mode with frequency, as shown in Fig. 3.8. In the low-frequency region, high resistivity due to the dominance of grain boundaries is experienced because of the high energy requirement in electron hopping. In the high-frequency area, the

dominant effect of grain reduces resistivity by decreasing the required energy for electron hopping, causing a decreasing pattern of tanδ.

3.2.7 Electrical Properties

The variation of ac-resistivity is shown in Fig. 3.9, and their values at 1 MHz frequency are given in Table 3.5. It is observed that the resistivity is found to increase with Co content. The ac-resistivity is indirectly proportional to the dielectric constant and tangent loss. A decreasing trend of ε and $tan\delta$ in the Co-substituted sample may be the reason for the obtained resistivity pattern. The improvement in resistivity may also result from the creation of more number of closed porosity due to the presence of low melting cobalt (Kaur et al., 2005). Ferrite conductivity is governed by the electron hopping between Fe^{2+} and Fe^{3+}. The Co ions generally occupy the octahedral site of Fe ions and increase Fe^{2+} ions at tetrahedral sites by decreasing the number of Fe^{3+} at the octahedral site. It weakens the oxygen-coupled exchange interaction of Fe ions. Also, spin canting, magneto-transport effect, cation migration, etc. are responsible for such kinds of ac-resistivity behavior.

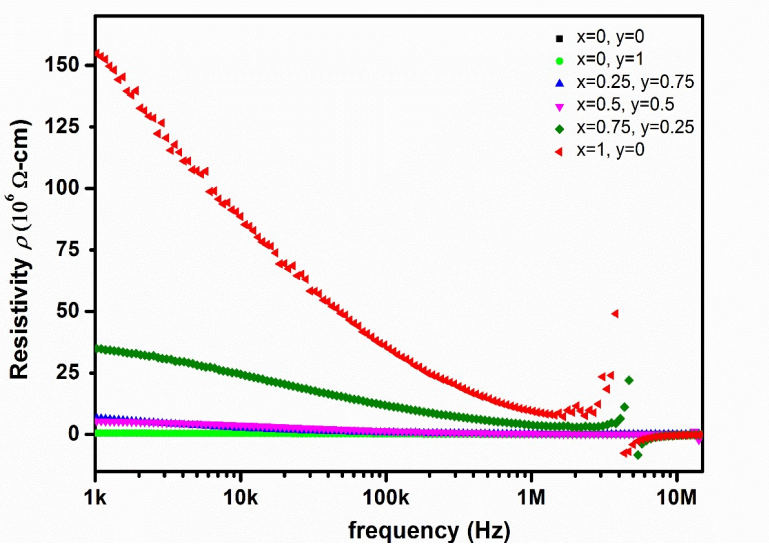

Figure 3.9 *Ac-resistivity (ρ) of $SrFe_{12-x-y}Co_xCr_yO_{19}$ ($0 \leq x, y \leq 1$) hexaferrites with respect to frequency.*

3.3 Conclusions

$SrFe_{12-(x+y)}Co_xCr_yO_{19}$ (x, y = 0,0; 0,1; 0.25,0.75; 0.50,0.50; 0.75,0.25; 1,0) were successfully synthesized by the sol-gel auto-combustion process. Structural, magnetic, dielectric, and electrical studies were carried out to see the substitutional effect of Co and Cr ions. Substitution of Co ion is found favorable to improve M_s value with a drastic decrease in H_c. In contrast, Cr ion is observed to significantly enhance H_c value without adversely affecting the M_s value. $SrFe_{11}Co_{0.75}Cr_{0.25}O_{19}$ (70.08 emu/g) and $SrFe_{11}CoO_{19}$ (71.18 emu/g) compositions have shown a good improvement in M_s of SrM hexaferrite. In $SrFe_{11}CrO_{19}$, M_s of 59.89 emu/g and H_c of 6.26 kOe are obtained. Such improvements in SrM can make it possible to approach the various application area of the permanent magnet. Also, it brings up innovative research challenges for the development of more proficient and more powerful non-rare-earth magnets.